A Correlation for the Characteristic Velocity Ratio to Predict Hydrodynamics of Capillary Gas–Liquid Taylor Flow[1]

Martin Wörner*

Karlsruhe Institute of Technology (KIT), Institute for Catalysis Research and Technology, Karlsruhe, 76131 Germany
**e-mail: martin.woerner@kit.edu*

Abstract—The ratio between bubble velocity and mean velocity of the two-phase flow is a key parameter in Taylor flow. Correlations for this characteristic velocity ratio that are valid over the entire range of attainable capillary numbers are missing so far. Here, we develop such a correlation for laminar gas–liquid Taylor flow in circular capillary channels. The proposed model is a two-parameter logistic function, which approaches the theoretical asymptotic limit of Bretherton at low capillary number. The correlation relies on prior known parameters such as channel diameter, fluid properties and gas/liquid volumetric flow rates only. In comparison with numerical and experimental data, it is accurate within ±5 and ±18%, respectively. The correlation should be useful to estimate various prior unknown hydrodynamics features of Taylor flow such as bubble velocity, mean liquid velocity, gas holdup, uniform liquid film thickness, bubble diameter, and streamline patterns in the liquid slug. The derived two-parameter logistic function may be useful to develop similar correlations for non-circular channels and liquid–liquid Taylor flow.

INTRODUCTION

Taylor flow is a special kind of slug flow in small channels, where the liquid slugs separating the elongated bullet-shaped bubbles (Taylor bubbles) are free from gas entrainment. This flow regime, which is also known as bubble train flow, segmented flow or capillary slug flow, occurs in microfluidic devices for applications in life sciences (lab-on-a-chip), material synthesis and chemical process engineering, e.g. in heat exchangers and catalytic multiphase capillary and monolithic reactors [1]. Among the various gas-liquid flow patterns in microchannels [2], Taylor flow is attractive because of its well-defined interfaces and flow conditions, which are easier to control than in macroscopic devices and because of its advantageous mass transfer properties. The latter stems from (i) the high interfacial area per unit volume, (ii) the thin liquid film that separates the gas bubble from the channel wall, and (iii) the recirculation in the liquid slug, which accounts for good mixing and a wall-normal convective transport in laminar flow [3]. For recent reviews on Taylor flow we refer to [4–7].

The shape of the Taylor bubble depends mainly on the (bubble) capillary number $Ca_b = u_b \mu_L / \sigma$ and to a lesser extent on the Reynolds number $Re_b = \rho_L u_b D / \mu_L$. Here, u_b denotes bubble velocity, ρ_L liquid density, μ_L liquid viscosity, σ surface tension and D the pipe diameter. At low Ca_b, both bubble ends form hemispherical caps connected by a uniform cylindrical section of radius R_b [8]. As Ca_b increases, the Taylor bubble gets more slender and the fore-aft symmetry is lost. In addition, there are capillary wave undulations where the uniform interface merges with the transition region in the rear [9]. The curvature of the bubble nose increases approaching a limiting value at $Ca_b = O(1)$. The profile of the rear transition undertakes large deformations as its shape evolves from convex for small values of Ca_b to concave at large values of Ca_b [10]. For high bubble speeds, the trailing end develops re-entrant cavities of the continuous liquid phase [11] which cause bubble breakup at capillary numbers of order one and above [12, 13].

Of primary interest for many applications with Taylor flow is the thickness of the uniform liquid film $\delta = R - R_b$. Several correlations have been suggested in the literature to relate δ with Ca_b, see below. For engineering practice, the direct benefit of these correlations is at first limited as the bubble velocity and thus Ca_b are not prior known in general. Often mass flow controllers serve to prescribe the gas and liquid flow rates Q_G and Q_L. For a straight channel with constant cross-section A, thus the superficial velocities $j_G = Q_G/A$ and $j_L = Q_L/A$, the total superficial velocity (or total volumetric flux) $j_T = j_G + j_L$ and the volumetric flow rate ratio (dynamic holdup) $\beta = Q_G/(Q_G + Q_L) =$

j_G/j_T are known. In contrast, the mean gas velocity u_G and the void fraction $\alpha = j_G/u_G$ are unknown. In small channel Taylor flow, liquid slugs are usually free from gas entrainment to that $u_b = u_G$. Thus, Ca_b is unknown as well. Particularly useful for practical applications of Taylor flow would be a (preferentially) universal correlation that relates the bubble velocity, the liquid film thickness and other important hydrodynamic parameters of Taylor flow to the total superficial velocity j_T. The purpose of the present paper is to develop such a correlation and to embed it in a unifying theoretical framework for characterization of Taylor flow hydrodynamics. Here we restrict our study to laminar gas-liquid Taylor flow through a straight circular pipe where the diameter is sufficiently low so that gravitational effects are negligible.

We formulate the desired correlation for the ratio between the (unknown) bubble velocity u_b and the (known) mean velocity of the two-phase flow, i.e. the total superficial velocity j_T. For two incompressible phases, the mean axial velocity in the liquid slug (u_s) equals j_T [14]. Several researchers indicated the fundamental importance of this velocity ratio for Taylor flow [7, 14, 15]. Here, we denote $\eta = u_b/j_T$ as the characteristic velocity ratio of Taylor flow. Since the proposed correlation for η is formulated in terms of prior known parameters only, it may also serve as closure relation for mechanistic models of Taylor flow in complement to closure relations for the Taylor bubble rise velocity proposed for larger channels [16].

The organization of the paper is as follows. We first give some fundamental relations in capillary Taylor flow. Thereafter, we summarize the state of the art in literature to elucidate the functional dependence of η on the (two-phase) capillary number $Ca = j_T\mu_L/\sigma$, which is based on j_T as velocity scale. As main part, we present the development of the new model and its evaluation with respect to recent experimental and numerical data from literature. This is followed by a discussion of the accuracy, limitations and benefit of the model for predicting hydrodynamics of Taylor flow.

FUNDAMENTAL RELATIONS IN CAPILLARY TAYLOR FLOW

Conditions and Assumptions

We consider the laminar pressure-driven gas-liquid flow through a cylindrical horizontal capillary (radius R, diameter $D = 2R$, cross-sectional area $A = \pi R^2$). Both phases are incompressible and immiscible Newtonian fluids. We assume that the gas density ρ_G, the liquid density ρ_L, the gas viscosity μ_G, the liquid viscosity μ_L and the coefficient of surface tension σ are all constant.

The importance of gravitational and buoyancy effects is usually quantified by the Eötvös number $Eo = g(\rho_L - \rho_G)D^2/\sigma$ or by the Bond number $Bo =$ $g\rho_L D^2/\sigma$. Leung et al. [17] experimentally studied the effect of gravity in horizontal gas-liquid Taylor flow in three different millimeter-sized channels ($D = 1.12$, 1.69, 2.12 mm giving Eo = 0.287, 0.653 and 1.028). The authors observed gravity-induced drainage flow from the top to the bottom of the pipe within the liquid film resulting in bubble asymmetry. However, these effects diminish for small values of Eo and/or Ca. Magnini et al. [18] systematically investigated the effect of buoyancy on the Taylor bubble shape and velocity in vertical tubes by experiments and numerical simulations. The authors showed that buoyancy could have a notable effect even at Bond numbers below unity. Here we assume that the channel size is so small that gravity/buoyancy effects are negligible (Eo → 0), a criterion that should be fulfilled for submillimeter channels. Accordingly, the bubble profile and the flow field are assumed axisymmetric and steady in a frame of reference moving with the bubble.

We further assume that the liquid slugs of Taylor flow are sufficiently long to form a fully developed parabolic velocity profile so that there is no interaction between neighboring bubbles. In addition, the bubble is assumed to be sufficiently long so that there is a region where the bubble has a cylindrical shape with the thickness of the liquid film being uniform and independent of bubble length as described in [19]. Such a situation occurs when the front and the back of the bubble are virtually independent. The inertia-free boundary integral computations of Lac and Sherwood [13] suggest that this is the case when the ratio between the radii of the undeformed bubble and the tube exceeds a value of 1.1. A further quantitative criterion for the minimum bubble length (relative to tube radius) in terms of Ca_b in absence of inertia and gravity is given in [20]. In the presence of inertia, the necessary bubble length to form a uniform film region steeply increases with Re_b, in particular at high Ca_b [9]. Fig. 1 shows a sketch of the Taylor flow configuration under analysis with characteristic parameters. Real images of such Taylor bubbles can be found e.g. in reference [21].

Mass Balance

A global mass balance for the two-phase flow yields [14, 22]

$$\underbrace{u_f A_f}_{=Q_f} + \underbrace{u_b A_b}_{=Q_b} = \underbrace{j_T A}_{=Q_s}. \tag{1}$$

Here, u_f is the mean axial velocity of the liquid in the uniform film region while $A_f = \pi(R^2 - R_b^2)$ and $A_b = \pi R_b^2$ denote the cross-sectional area of the film and the bubble in this region, respectively.
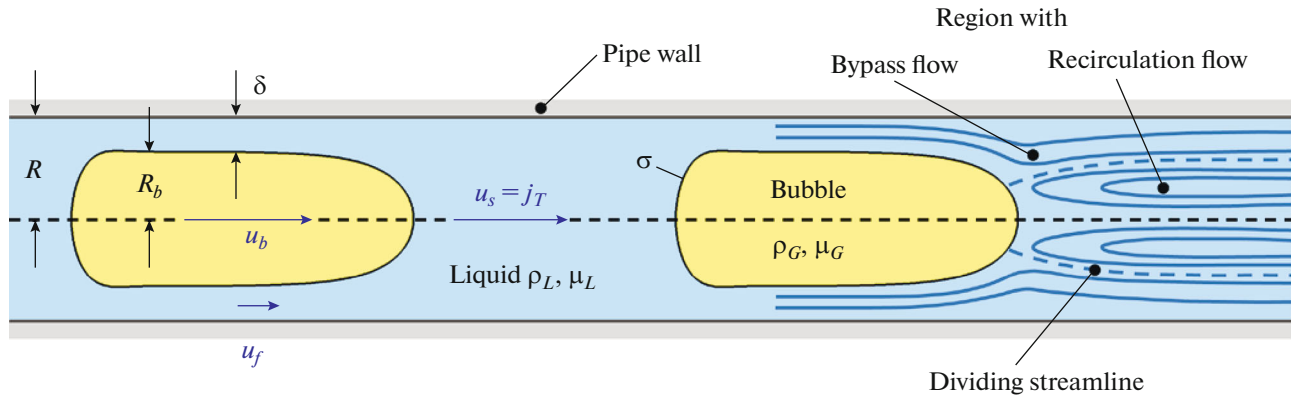
Fig. 1. Sketch of axisymmetric Taylor flow in a circular pipe (radius R) with streamline patterns and important parameter.

For a compact notation, we introduce the wetting fraction

$$w = \frac{A_f}{A} = 1 - \frac{R_b^2}{R^2} = 1 - \left(1 - \frac{\delta}{R}\right)^2 = \frac{2\delta}{R}\left(1 - \frac{\delta}{2R}\right). \quad (2)$$

This quantity is of interest for the penetration of a gas phase into a capillary where it displaces a viscous liquid [23]. When gravitational forces are negligible, the thickness of the liquid film deposited at the wall becomes constant in a distance sufficiently far from the bubble tip [8, 24]. The relative cross-sectional area fraction $w = A_f/A$ then represents the fraction of liquid left behind the bubble. In terms of the wetting fraction, Eq. (1) can be expressed as

$$\frac{u_b}{j_T} = \frac{1}{1 - w}\frac{1}{1 + Q_f/Q_b}, \quad (3)$$

a relation that will be useful later.

As further quantity of interest, we define the relative drift velocity

$$m = \frac{u_b - j_T}{u_b} = 1 - \frac{j_T}{u_b}. \quad (4)$$

From Eq. (3) it follows

$$m = 1 - (1 - w)\left(1 + \frac{Q_f}{Q_b}\right). \quad (5)$$

For a liquid film at rest it is $Q_f = u_f = 0$ and Eq. (5) yields

$$m = w = 1 - \frac{R_b^2}{R^2} = \frac{2\delta}{R}\left(1 - \frac{\delta}{2R}\right). \quad (6)$$

Such a stagnant liquid film with zero velocity occurs in the constant film thickness region of inviscid bubbles that cannot exert tangential stresses [11]. In studies on the displacement of a viscous liquid in a capillary by the steady propagation of an inviscid semi-infinite finger [8, 25−27] or by a long inviscid bubble [28] m and w are often used synonymously.

Streamline Patterns in Liquid Slug

For gas-liquid mass transfer in Taylor flow, the streamline patterns in the liquid slug are of great importance [5]. These can be classified in recirculating flow (see sketch in Fig. 1) and complete bypass flow, resulting in different pathways for mass-transfer.

In a frame of reference moving with the Taylor bubble a recirculation pattern in the liquid slug occurs when the bubble velocity is lower than the liquid velocity on the channel axis, i.e. for $u_b < u_{L,\max}$ [23, 29]. For a liquid slug with a laminar fully developed parabolic velocity profile the maximum liquid velocity is given by $u_{L,\max} = 2j_T$. Thus, for $m < 0.5$ streamline patterns show a recirculation region whereas for $m > 0.5$ complete bypass flow (CBF) occurs [11].

The cross-sectional regions with recirculation flow (in the channel center) and partial bypass flow (close to the walls) are separated by the dividing streamline [30], see Fig. 1. The position of the dividing streamline results from the condition that the axial flow rate in the recirculation area is zero in the moving frame of reference. The radial position of the dividing streamline (R_{ds}) and the radial position where the velocity in the moving frame of reference is zero (R_0) are given by [30]

$$\frac{R_{ds}}{R} = \frac{\sqrt{2}R_0}{R} = (2 - \eta)^{1/2}. \quad (7)$$

Thus, the relative cross-sectional area of the recirculation region is $A_{ds}/A = 2 - \eta$.

The intensity of the recirculation can be quantified by the time needed for the liquid to move from one end of the liquid slug to the other end. A second characteristic time scale is the time needed by the liquid slug to travel a distance of its own length. Thulasidas et al. [30] used the ratio of both time scales to define a non-dimensional recirculation time. For a circular channel the non-dimensional recirculation time is [31]

$$\tau = \left(\frac{1}{\eta} - \frac{1}{2}\right)^{-1}. \quad (8)$$

LITERATURE RELATIONS FOR FILM THICKNESS AND BUBBLE VELOCITY

In this section, we summarize relations on the liquid film thickness and bubble velocity, which we will utilize in the subsequent section for the development of the new model.

Liquid Film Thickness

In his classical paper [24], Bretherton applied lubrication theory to the flow in the liquid film to derive the first theoretical expression for the film thickness. Using only local conditions at the bubble nose, the asymptotic film thickness is independent of bubble length and given by

$$\frac{\delta_{Br}}{R} = 0.643(3Ca_b)^{2/3} = \underbrace{1.3375}_{=P}Ca_b^{2/3}. \qquad (9)$$

Eq. (9) is only valid for very low capillary and Reynolds numbers and according to Bretherton's own experiments accurate within 10% for $Ca_b < 5 \times 10^{-3}$.

By a scaling analysis, Aussilious and Quere (AQ) [32] derived the following equation for the liquid film thickness of a semi-infinite bubble in a circular tube

$$\frac{\delta_{AQ}}{R} = \frac{P \cdot Ca_b^{2/3}}{1 + \underbrace{2.5}_{=F} \times P \cdot Ca_b^{2/3}} = \frac{1.3375Ca_b^{2/3}}{1 + 3.344Ca_b^{2/3}}. \qquad (10)$$

The factor $F = 2.5$ is obtained empirically by fitting experimental data of Taylor [23]. This relation is valid in the range $10^{-3} \leq Ca_b \leq 1.4$ and approximates Eq. (9) for small capillary numbers. Klaseboer et al. [33] presented an analytical extension of Bretherton's work yielding an expression identical to Eq. (10), except $F = F_{KGM} = 2.79$. Balestra, Zhu and Gallaire (BZG) [34] performed an extensive computational study on the hydrodynamics of Taylor bubbles and drops in capillaries under negligible gravity focusing on the effect of the viscosity ratio $\lambda = \mu_G/\mu_L$. Using COMSOL Multiphysics, they solved the Stokes equations by a moving mesh method for capillary numbers in the range $10^{-4} \leq Ca \leq 1$. By fitting the numerical results for a bubble $(\lambda = 0)$, they found $F = F_{BZG} = 2.483$ which is close to the value of AQ [32].

Eq. (10) neglects inertial effects, which can become important at higher velocities causing a non-monotonic dependence of the film thickness on the Reynolds number in a circular tube [8, 35] or a two-dimensional channel [36]. Han and Shikazono [37] proposed the correlation

$$\frac{\delta_{HS}}{R} = \frac{0.643(3Ca_b)^{2/3}}{1 + 3.13Ca_b^{2/3} + 0.504Ca_b^{0.672}Re_b^{0.589} - 0.352We_b^{0.629}} = 0.643f_{HS}, \qquad (11)$$

which accounts for inertial effects by Re_b and the Weber number $We_b = Ca_bRe_b$. Eq. (11) was derived from film thicknesses measurements for water and ethanol with $0 < Ca_b < 0.4$ and $0 < Re_b < 2000$. Howard and Walsh [7] found that this correlation predicts the film thickness best at higher capillary numbers amongst the existing correlations.

Langewisch and Buongiorno (LB) [38] studied capillary Taylor flow numerically with Ca and Re in the ranges $0.005-0.2$ and $0-900$, respectively. The density ratio was fixed to 0.001 and the viscosity ratio to $\lambda = 0.01$ while gravity is neglected. The authors proposed the following model for the film thickness

$$\frac{\delta_{LB}}{R} = \frac{1.3375Ca^{2/3}}{1 + 2.86[1 + \Phi(Re)]Ca^{0.764}}, \qquad (12)$$

where

$$\Phi(Re) = \begin{cases} 0 & Re = 0 \\ \left(\dfrac{32.05}{Re^{0.593}} + 4.564 \times 10^{-5}Re^{1.909}\right)^{-1} & Re > 0 \end{cases} \qquad (13)$$

Here, $Ca = Ca_b/\eta$ and $Re = Re_b/\eta$ represent the capillary and Reynolds number using j_T as characteristic velocity scale, respectively. Kurimoto et al. [39] found that the film thickness model of LB [38] shows a better agreement with their numerical results as compared to the model of Han and Shikazono [37].

Bubble Velocity

Literature relations for the bubble velocity are usually formulated either in terms of m or η. By the definition of m in Eq. (4), it is $\eta = 1 - m^{-1}$ so that both formulations are convertible.

Bretherton's [24] analytical approach at low Ca_b resulted in the expression

$$m = 1.29(3Ca_b)^{2/3} = 2.683Ca_b^{2/3}, \qquad (14)$$

corresponding to

$$\eta = \frac{1}{1 - m} \approx 1 + m = 1 + 1.29(3Ca_b)^{2/3}. \qquad (15)$$

Giavedoni and Saita [8] found that their numerical results for the film thickness match the theoretical correlation of Bretherton for $Ca_b < 10^{-3}$. Fairbrother and Stubbs [40] suggested the empirical correlation
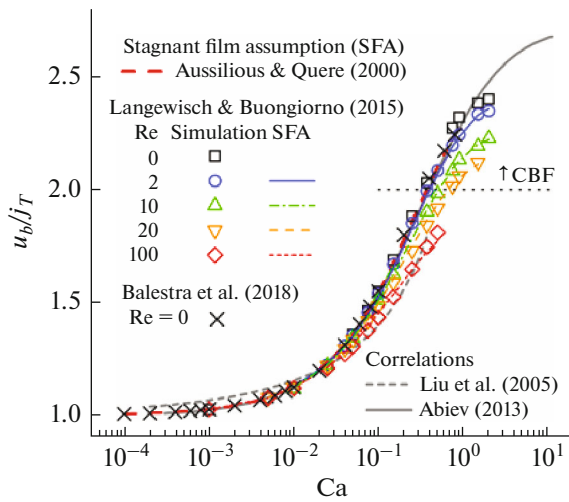
$$m = Ca_b^{1/2}, \qquad (16)$$

Fig. 2. Dependence of characteristic velocity ratio on capillary number and Reynolds number from various sources [32, 34, 38, 41, 43].

different liquids in co-current upward flow. They fitted their experimental data for the ratio of bubble velocity to total superficial velocity by the correlation

$$\frac{u_b}{j_T} = \frac{1}{1 - 0.61\mathrm{Ca}^{0.33}}, \quad (18)$$

which is valid in the range $2 \times 10^{-4} \le \mathrm{Ca} \le 0.39$.

Abiev [22] developed a mathematical model for the bubble velocity and validated it by experimental data from literature [30, 42]. Based on calculations with this model, he proposed the following approximation for horizontal flow [43]

$$\frac{u_b}{j_T} = 1 + 1.716\left[1 - \exp\left(-f_{\mathrm{Abiev}}(\mathrm{Ca}_b)\right)\right], \quad (19)$$

where

$$f_{\mathrm{Abiev}}(\mathrm{Ca}_b) \quad (20)$$
$$= \exp\left[-0.0204 + 0.4714\ln\mathrm{Ca}_b - 0.0211(\ln\mathrm{Ca}_b)^2\right].$$

This relation is valid in the range $10^{-4} \le \mathrm{Ca}_b \le 50$.

The Taylor bubble velocity in slug flow is often modelled based on the drift flux approach [44, 45] which reads

$$u_b = C_0 j_T + u_d. \quad (21)$$

Here, C_0 is the distribution parameter and u_d is the drift velocity. The drift velocity is regarded zero in horizontal microchannels. With $u_b = j_G/\alpha$ and $j_T = j_G/\beta$ Eq. (21) then yields the relation

$$\eta = \frac{u_b}{j_T} = \frac{\beta}{\alpha} = C_0. \quad (22)$$

In microchannels, the characteristic velocity ratio thus takes the role of the distribution parameter.

From a large number of experiments, Kurimoto et al. [21] proposed the following model for the distribution parameter

which is valid in the range $7.5 \times 10^{-5} < Ca_b < 0.014$. Experiments for very viscous fluids in 1.5−3 mm circular tubes by Taylor [23] indicate that the validity of Eq. (16) may be extended up to $Ca_b = 0.09$. Taylors experimental data up to $Ca_b = 2$ are well fitted by inserting the film thickness model of AQ [32] for a stagnant liquid film ($m = w$) into Eq. (2) giving

$$m = 1 - \left(1 - \frac{\delta_{\mathrm{AQ}}}{R}\right)^2 = 1 - \left(1 - \frac{P\mathrm{Ca}_b^{2/3}}{1 + FP\mathrm{Ca}_b^{2/3}}\right)^2. \quad (17)$$

For large capillary numbers, m adopts an asymptotic value, see discussion below.

Liu et al. [41] performed experiments in capillaries with circular and square cross-section with hydraulic diameters in the range of 0.9−3 mm using air and three

$$C_0 = 1 + \sqrt{\mathrm{We}_b\left[7.18 \times 10^{-4} + 2.91 \times \mathrm{Re}^{-0.875}(1 - 0.845)\mathrm{Re}^{0.0259}\right]}/f_{\mathrm{HS}}, \quad (23)$$

where f_{HS} is defined in Eq. (11). This correlation has the disadvantage, that both, u_b and j_T must be known in order to evaluate We_b and Re. Thus, an iterative procedure is required, which may hinder a broader practical application of this model.

A NEW CORRELATION FOR THE CHARACTERISTIC VELOCITY RATIO

The goal of this paper is to derive a simple yet accurate correlation for the characteristic velocity ratio $\eta = u_b/j_T$ in terms of prior known non-dimensional parameters. Suo and Griffith [14] performed a dimensional analysis and obtained seven independent dimensionless groups. Here, the ratios of liquid-to-gas

density and viscosity as well as the ratios of bubble and liquid slug length to tube diameter are all assumed large being without influence while gravity is negligible (cf. Section Conditions and Assumptions). The two remaining parameters from the dimensional analysis in [14] are the capillary number and the Ohnesorge number. As the latter can be expressed in terms of capillary number and Reynolds number, we base our correlation for η on Ca and Re.

Evaluation of Literature Data

To develop a new model we evaluate the information from literature collected in the previous section. For that purpose, we plot in Fig. 2 various relations for η as function of Ca. The correlation of Liu et al. [41]
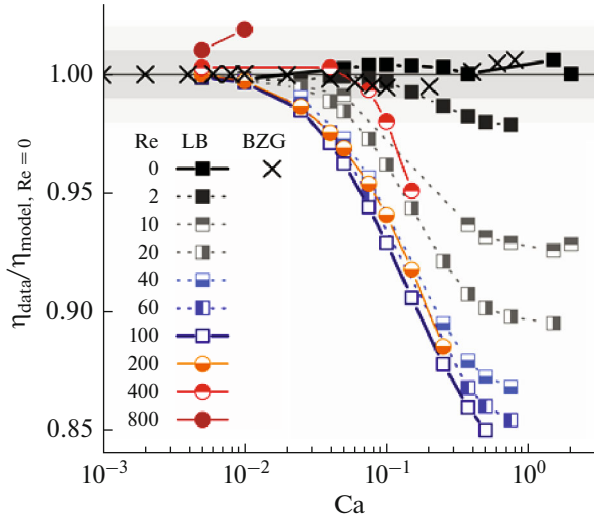
Fig. 3. Normalization of η data from numerical simulations [34, 38] by Eq. (36), representing the present model for vanishing Reynolds number.

in Eq. (18) is an explicit relation of the form $\eta = \eta\,(\mathrm{Ca})$ and can be plotted without further processing.

The correlation of Abiev [22] in Eq. (19) is an implicit relation between η and Ca. Since we could not bring it in an explicit form, we evaluate it as follows. For a given set of values for Ca_b we compute by Eq. (19) the corresponding values of η and thereafter the corresponding values of $\mathrm{Ca} = \mathrm{Ca}_b/\eta$. This procedure yields the relation $\eta = \eta(\mathrm{Ca})$ plotted in Fig. 2.

Next, we utilize correlations for the relative velocity *m*. By inserting relations for *m* into Eq. (4), one can evaluate the velocity ratio. In this way, we obtain by insertion of Eq. (17) the result

$$
\eta = \left(1 - \frac{P\mathrm{Ca}_b^{2/3}}{1 + FP\mathrm{Ca}_b^{2/3}}\right)^{-2}
$$
$$
= \left(1 - \frac{P\eta^{2/3}\mathrm{Ca}^{2/3}}{1 + FP\eta^{2/3}\mathrm{Ca}^{2/3}}\right)^{-2}. \tag{24}
$$

Eq. (24) represents again an implicit relation between η and Ca. Here we take $F = F_{\mathrm{AQ}} = 2.5$ and proceed as described above to plot it in Fig. 2. Similarly, we inserted and evaluated Eq. (14) of Bretherton [24] which is valid at low capillary numbers only. The corresponding graph overlaps with Eq. (24) and is not included in Fig. 2.

We now utilize correlations for the liquid film thickness to evaluate the characteristic velocity ratio. In gas-liquid Taylor flow, the viscosity ratio is typically very small resulting in negligible velocity in the liquid film. From Eq. (6) one obtains the relation

$$
\eta = \frac{1}{1-w} = \frac{R^2}{R_b^2} = \left(1 - \frac{\delta}{R}\right)^{-2}. \tag{25}
$$

Thus, one can determine the velocity ratio from correlations for δ or R_b. Inserting the film thickness model of AQ [32] given in Eq. (10) into Eq. (25) yields Eq. (24). The film thickness models of LB [38] in Eq. (12) accounts for inertial effects by the Reynold number Re. Inserting Eq. (12) in Eq. (25) yields an explicit relation $\eta = \eta(\mathrm{Ca}, \mathrm{Re})$ which is plotted by the thin lines in Fig. 2 for various values of Re. This model has the disadvantage that the function $\Phi(\mathrm{Re} = 0)$ in Eq. (13) is discontinuous at Re = 0. The film thickness model of Han and Shikazono [37] accounts for inertial effects by the Reynolds number Re_b and the Weber number $\mathrm{We}_b = \mathrm{Ca}_b\mathrm{Re}_b$. Inserting Eq. (11) in Eq. (25) yields together with $\mathrm{We}_b = \eta^2\mathrm{CaRe}$ again an implicit relation of the form $\eta = \eta(\mathrm{Ca}, \mathrm{Re})$, which is however not evaluated here.

Included in Fig. 2 are numerical data from two recent numerical studies with state of the art CFD simulations (symbols). The results of BZG [34] for Re = 0 cover 20 distinct values of Ca in the range 0.0001−0.8 (taken from Fig. 16a in [34]). The numerical results of LB [38] cover 14 distinct values of Ca in the range $0.005 \le \mathrm{Ca} \le 2$ at various values of Re. In Fig. 2, only data for Re = 0, 2, 10, 20 and 100 are included while results for Re > 100 will be discussed in Fig. 3 below.

We now discuss Fig. 2 displaying the various data and relationships. All relations and data show a monotonic increase of η with Ca. With exception of the model of Liu et al. [41] in Eq. (18), all data virtually overlap for Ca < 0.02. In this range, η is close to unity indicating that the bubble moves only slightly faster than the total superficial velocity. The curve resulting from the film thickness model of AQ [32] in combination with the stagnant film assumption (SFA) is in the entire range of Ca in excellent agreement with the model of Abiev [43]. The same holds for the numerical data of LB [38] for Re = 0 and 2 in the range $0.005 \le \mathrm{Ca} \le 1$. Only the two data points at Ca = 1.5 and 2 show slightly lower values of η as compared to the model of Abiev [43]. For the larger values of Re, the numerical data of LB [38] show a continuous decrease of η with increase of Re. The viscosity ratio in the numerical simulations of LB [38] is λ = 0.01. The thin lines in Fig. 2 represent the film thickness model of LB [38] in combination with the stagnant film assumption for λ = 0. For Re ≤ 20, the lines agree very well with the numerical data, which indicates that the assumption of a stagnant liquid film is a reasonable approximation. For Re = 100, however, a slight deviation exists especially at large values of Ca.

Flows with Negligible Inertia

As a strategy for the development of our new model we first consider the limit Re = 0 and then introduce the effect of finite Re. The model development for vanishing Reynolds number relies on the principle of

mass conservation, which we aim to combine with information from momentum equation.

Equation (3), which results from a global mass balance, shows that the characteristic velocity ratio u_b/j_T depends on the flow rate of the liquid film. Depending on the gas-to-liquid viscosity ratio $\lambda = \mu_G/\mu_L$, the liquid film may be stagnant ($\lambda \to 0$) or be carried along by shear forces. Estimating the flow rate in the liquid film requires a momentum balance. To that end, one may approximate the uniform body of the bubble by a long concentric cylinder surrounded by an annular liquid film. Under the further assumption that the flow in both phases is fully developed and laminar, the radial profiles for the local velocity within the concentric gas core and the annular liquid film can be computed analytically [46, 47]. These velocity profiles are an important ingredient in the model of Abiev [22]. For the ratio of flow rates, it follows [14]

$$\frac{Q_b}{Q_f} = \frac{1-w}{w}\left(2 + \frac{1}{\lambda}\frac{1-w}{w}\right). \qquad (26)$$

Inserting Eq. (26) in Eq. (3) yields after some algebraic manipulations

$$\eta = \frac{1 - w(1 - 2\lambda)}{1 - (2w - w^2)(1 - \lambda)}. \qquad (27)$$

In the literature, various forms of this relation exist. Eq. (27) is equivalent to Eq. (16) in [14], to Eq. (12) in [7] and to Eq. (32) in [34]. It is also equivalent to Eq. (5) in [48], with reference to earlier work in [11]. In the limit $\lambda \to 0$, Eq. (27) reduces to Eq. (25).

With j_T and λ given, Eq. (27) forms a system of two unknowns (u_b and w) which one cannot solve analytically. By Eq. (2), w may be replaced by the bubble radius R_b or the liquid film thickness δ. Balestra et al. [34] combined Eq. (27) with a AQ-type film thickness model and solved the system for different values of the viscosity ratio λ numerically. More recently, Makuch et al. [48] performed a similar approach based on the Bretherton film thickness model in Eq. (9) extended for nonzero λ. The authors fitted the numerical results by a scaling function establishing an algebraic relationship valid for low values of Ca_b.

Here, we solve Eq. (27) in combination with the AQ [32] film thickness model in Eq. (10) numerically using the Matlab script provided by BZG [34] as supplemental material. Considering the viscosity ratio $\lambda = 0$ and different values of F proposed in literature, we obtained in this way graphs for the velocity ratio $\eta = \eta$ (Ca) for the range $10^{-5} \le Ca \le 10^3$. While values $Ca \gg 1$ may not represent physically stable Taylor flow as discussed below, the curves show some interesting features, which are useful for model development. With two distinct asymptotic limits $Ca \to 0$ and $Ca \to \infty$, the curves η (Ca) are of sigmoidal type and symmetric with respect to the inflection point. The lower asymptotic limit is $\eta_0 = \eta$ (Ca $\to 0$) = 1 while the upper

asymptotic limit $\eta_\infty = \eta$ (Ca$\to\infty$) depends on the value of F.

By virtue of Eq. (4), the existence of an upper asymptotic limit η_∞ for large capillary numbers is consistent with the asymptotic value for the relative drift velocity m. The value $m_\infty = 0.56$ reported by Taylor [23] for $Ca_b = 2$ corresponds to $\eta_\infty = 2.27$. In experiments at a viscosity ratio $\lambda = 2.5 \times 10^{-5}$, Cox [49] considered capillary numbers up to $Ca_b = 10$ and reported a slightly higher asymptotic value $m_\infty = 0.60$ corresponding to $\eta_\infty = 2.5$. From boundary integral simulations for an inviscid bubble in creeping flow, Martinez and Udell [28] obtained the value $m_\infty = 0.59$ for $Ca_b = 10$ corresponding to $\eta_\infty = 2.44$. In a similar but more recent study, Lac and Sherwood [13] found an absolute maximal bubble velocity corresponding to $\eta_\infty = 2.5$ when Ca becomes very large. The same value was reported by Dupont et al. [50] from volume of fluid computations.

Being valid under the assumptions of a stagnant liquid film and negligible inertia, Eq. (24) yields in the limit $Ca \to \infty$ the relation

$$\eta_\infty(\text{Re} \to 0)$$
$$= \lim_{Ca\to\infty}\left(\frac{FP\eta^{2/3}Ca^{2/3}}{(F-1)P\eta^{2/3}Ca^{2/3}}\right)^2 = \left(\frac{F}{F-1}\right)^2. \qquad (28)$$

Values reported in literature for F range from 2.483 [34] to 2.79 [33] resulting in $\eta_\infty = 2.8$ and 2.43 when inserted in Eq. (28), respectively. This and the values given above indicate a relatively large uncertainty for η_∞ even when inertia is negligible.

The numerical data of LB [38] in Fig. 2 suggest that the upper asymptotic limit η_∞ depends on Re. Furthermore, for any value of Re the relationship $\eta = \eta$ (Ca) is not symmetric with respect to the inflection point. To fit an asymmetric sigmoidal curve, a five-parameter logistic (5PL) function is required [51]. Here we adopt the 5PL function provided by the data analysis software Origin (OriginLab Corporation)

$$\eta_{5PL} = \eta_0 + \frac{\eta_\infty - \eta_0}{\left[1 + (Ca/c)^{-h}\right]^s}. \qquad (29)$$

The reason is that fitting by Eq. (29) shows better convergence as compared to the 5PL function proposed by Gottschalk and Dunn [51] when the focus is on low values of Ca as it is the case here. Fixing the lower asymptote to $\eta_0 = \eta(Ca \to 0) = 1$, four free parameters remain where we restrict the domain to $\eta_\infty > 1$, $c > 0$, $h > 0$ and $s > 0$.

To determine further of the four parameters, we consider the asymptotic limit of Bretherton in Eq. (15). For $Ca_b \to 0$, the velocity ratio approach

unity. Thus, for $Ca_b \to 0$ it follows $Ca \to Ca_b$ so that the asymptotic limit in Eq. (15) can also be written as

$$\eta \approx 1 + 1.29(3Ca)^{2/3}. \tag{30}$$

Our goal is to choose the parameters of the logistic function in such a way that the limit of Eq. (29) agrees with Bretherton's limit in Eq. (30). In the limit $Ca \to 0$ it is $(Ca/c)^{-h} \gg 1$ so that Eq. (29) may be approximated as

$$\eta \approx 1 + (\eta_\infty - 1)(Ca/c)^{hs}. \tag{31}$$

Comparing Eq. (30) and Eq. (31) shows that both limits become identical when $hs = 2/3$ and $(\eta_\infty - 1)\,c^{-2/3} = 1.29 \times 3^{2/3}$. With these two conditions, there remain only two free parameters of the logistic function, namely h or s and η_∞ or c. Here, we choose s and η_∞ as remaining free parameters. Thus we have $h = 2/(3s)$ while c follows from relation

$$c = \frac{1}{3}\left(\frac{\eta_\infty - 1}{1.29}\right)^{3/2}. \tag{32}$$

The logistic function from Eq. (29) then takes the form

$$\eta_{2PL} = 1 + \frac{\eta_\infty - 1}{\left[1 + \left(\frac{\eta_\infty - 1}{1.29}\right)^{1/s}(3Ca)^{-2/(3s)}\right]^s}. \tag{33}$$

For $s = 1$, Eq. (33) simplifies to

$$\eta_{1PL} = 1 + \frac{\eta_\infty - 1}{1 + \frac{\eta_\infty - 1}{1.29}(3Ca)^{-2/3}}. \tag{34}$$

with η_∞ being the sole free parameter. The function in Eq. (34) is symmetric with respect to the inflection point. For $F = F_{BZG} = 2.483$, Eq. (28) yields $\eta_\infty = 2.8$ so that Eq. (34) becomes

$$\eta = 1 + \frac{1.8}{1 + 0.6708Ca^{-2/3}}. \tag{35}$$

Eq. (35) is in good agreement with the AQ-SFA curve in Fig. 2 only for $Ca < 10^{-3}$.

A more accurate model for high values of Ca requires $s \neq 1$ in order to account for the asymmetric behavior. To determine appropriate values for s and η_∞ for the case of vanishing Reynolds number, we fit the data of LB [38] together with the data from Fig. 16a) in BZG [34] by function (33) using Origin. By regression analysis for in total 30 data points, we obtain $s(Re = 0) = 0.474$ and $\eta_\infty(Re = 0) = 2.467$. The latter value is well within the range reported in literature. Inserting both numerical values in Eq. (33) yields

$$\eta_{Re\to0} = 1 + \frac{1.467}{\left(1 + 0.280Ca^{-1.408}\right)^{0.474}}. \tag{36}$$

Eq. (36) constitutes the present model for vanishing Reynolds number.

Flows with Inertia

In order to estimate the accuracy of the new model for vanishing and finite Reynolds numbers, we normalize the numerical data of BZG [34] and LB [38] by Eq. (36). Figure 3 shows the corresponding ratio as function of Ca. For Re = 0, the difference between Eq. (36) and the numerical data is less than 1% over the entire range of Ca. For $Ca \le 0.01$, the deviation is virtually zero due to the fact that the asymptotic behavior agrees with the theory of Bretherton [24].

For Re = 2, the difference between Eq. (36) and the numerical data of LB [38] is less than about 2% over the entire range of Ca. For $Re \le 100$, the deviation is less than about 2% only for $Ca \le 0.025$. For larger values of Ca, the ratio in Fig. 3 decreases with increase of Re from 0 to 100. At a value of $Re \sim 100$, the ratio takes a minimum before it increases as Re increases up to 800.

Overall, Fig. 3 reveals that for the combination $Ca > 0.025$ and $Re > 2$ a refined model is required. Since for $Re \ge 200$ only few numerical data points are available, we restrict the development of an improved model to the range $0 < Re \le 100$. To that end, we follow the procedure from above and fit the numerical data of LB [38] for Re = 2, 10, 20, 40, 60 and 100 by Eq. (33) using Origin. By regression analysis, we obtain for each value of Re a combination of η_∞ and s. In all cases, the coefficient of determination of the regression is larger than 0.9996. This value is close to the theoretical maximum of unity, indicating that the present model fits the data very well.

In Fig. 4 we show the values of η_∞ and s for the above set of Re. In the range $20 \le Re \le 100$, the upper asymptote is about constant with $\eta_\infty \sim 2.3$. The exponent s, instead, is slightly increasing over the entire range of Re. Figure 4 shows that one can well approximate the dependence of both parameters on Re by relations

$$\eta_\infty(Re) = 2.3 + 0.167 \times 0.83^{Re} \tag{37}$$

and

$$s(Re) = 0.884 - 0.41 \times 0.968^{Re}. \tag{38}$$

Equations (33), (37) and (38) constitute the present new model which we expect to be valid for capillary numbers up to $Ca \sim 10$ and Reynolds numbers up to $Re \sim 100$.

DISCUSSION

Model Accuracy in Comparison with Literature Data

We assess the accuracy of the new model by a parity plot in Fig. 5 which compares the values of $\eta = \eta\,(Ca, Re)$ predicted by Eqs. (33), (37) and (38) with numerical data for η. The latter include in addition to the data from BZG [34] and LB [38] already used for model development the numerical data of Kurimoto et al. [39]. Figure 5 shows that for $Re \le 200$, the deviation
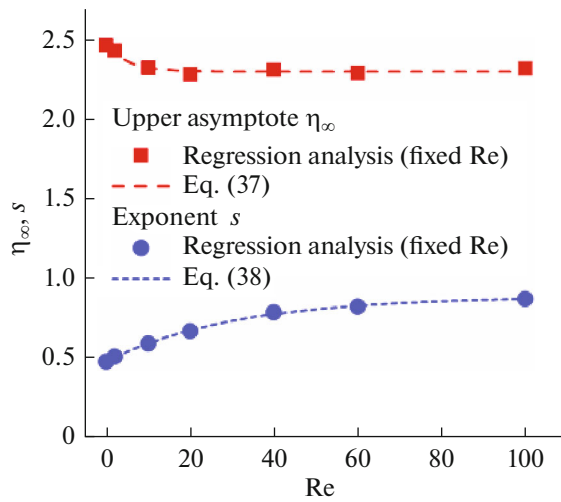
Fig. 4. Parameters η_∞ and s of the 2PL model versus Reynolds number.

Fig. 5. Parity plot comparing the present model with results from numerical simulations of Taylor flow [34, 38, 39].

between numerical data and model is within $\pm 2\%$ over the entire range of Ca. For Re = 200 and 400, the deviation is larger but still within $\pm 5\%$.

For further evaluation of the predictive capabilities of the new model, we show in Fig. 6 a second parity plot now comparing the model with the measurements listed in Table A1 of Kurimoto et al. [21]. The authors performed experiments in circular microchannels with four different diameters (D = 200, 320, 500, and 700 μm). They used three different liquids, namely water and two types of glycerol-water solutions with 64 and 52 wt % glycerol, respectively. The experiments encompass the ranges $0.005 \leq Ca_b \leq 0.235$ and $6 \leq Re \leq 941$ while η is in the range $1.1 - 1.6$. Concerning measurements accuracy, the author give a relative error for the measured gas slug volume, which was estimated as less than $\pm 3.0\%$.

The deviation between the present model and the experimental data in Fig. 6 is within $\pm 10\%$ for the diameter $D = 200$ μm. For the larger diameters $D = 320$ and 500 μm, the deviation is mostly in the range between 0 and -10%, meaning that the present model consistently underestimates the measurements. For the largest diameter $D = 700$ μm, the deviation is mostly in the range from -5 to -18%. Interestingly, the experiments with 52 wt % glycerol-water solution in the 200 μm channel is the only case were the present model consistently overestimates the measurements of Kurimoto et al. [21].

Limitations of Proposed Correlation

The comparison with experimental results in the previous subsection shows that the proposed model for the characteristic velocity ratio of Taylor flow may be considered sufficiently accurate with an error of $\pm 10\%$ for microchannels with diameter 500 μm and below
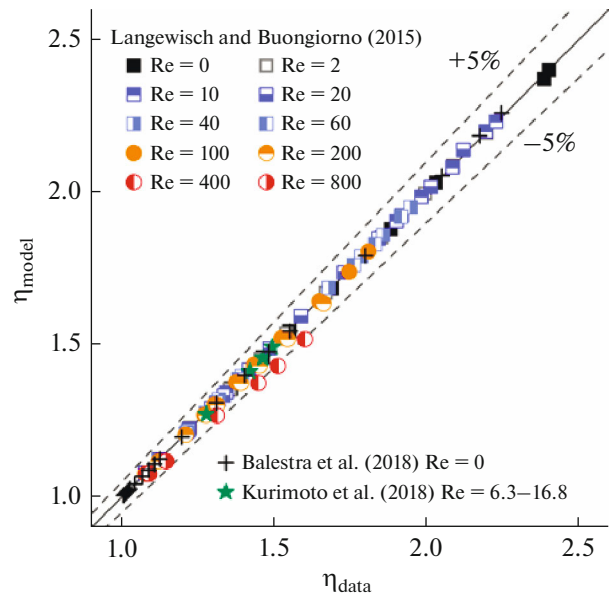
and Reynolds number up to Re ~ 400. For larger channel diameters and higher Reynolds numbers, the agreement is less good and refinement of the model is advisable.

The improvement of the model for high Reynolds number is hindered by the lack of reliable numerical and experimental data at large capillary numbers. Experimentally, it is quite hard to reach high Ca in capillaries (either by high velocities or by high viscosi-
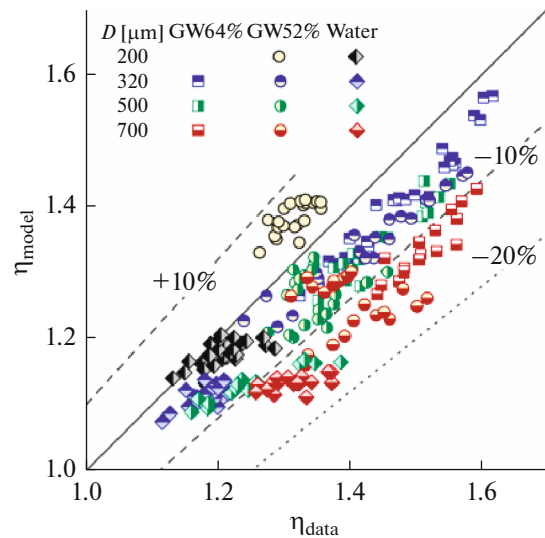

Fig. 6. Parity plot comparing the present model with the experiments of Kurimoto et al. [21]. In the experiments with glycerol-water (GW) solutions, Re is in the range $6-34.3$ (64 wt % glycerol) and $19.5-84.3$ (52 wt % glycerol). For water, Re is in the range $139-941$.

Table 1. Relations between priori unknown hydrodynamic parameters of Taylor flow and the characteristic velocity ratio

Unknown parameter	Relation
Void fraction and velocities	
Void fraction	$\alpha = \beta/\eta$
Bubble velocity	$u_b/j_T = \eta$
Mean liquid velocity	$u_L/j_T = (1 - \beta)/(1 - \beta/\eta)$
Slip ratio	$S = u_b/u_L = (\eta - \beta)/(1 - \beta)$
Relative drift velocity	$m = 1 - \eta^{-1}$
Relations for stagnant liquid film	
Uniform bubble radius	$R_b/R = \eta^{-1/2}$
Uniform film thickness	$\delta/R = 1 - \eta^{-1/2}$
Uniform wetting fraction	$w = 1 - \eta^{-1}$
Streamline patterns in liquid slug	
Condition for recirculation flow	$\eta < 2$
Radius of dividing streamline	$R_{ds}/R = (2 - \eta)^{1/2}$
Radius of vanishing velocity in moving frame	$R_0/R = (1 - \eta/2)^{1/2}$
Non-dimensional recirculation time	$\tau = 1/(\eta^{-1} - 0.5)$

ties) because it results in very high pressure-drops. While the utility of extending the model to large Ca may thus be limited for practical applications, it is nevertheless of academic interest.

The numerical simulations of LB [38] in Fig. 2 show that the value of η_∞ depends on Re. For Re ≤ 100 the upper asymptote decreases with increase of Re. For Re ≥ 200, there are not sufficient data available at large Ca to allow for a reliable regression analysis with respect to the upper asymptote, as the maximum values of Ca in the simulations of LB [38] decrease with increase of Re, cf Fig. 2. In fact, the upper asymptotic behavior of η at large Re seems to be largely unknown and a quantitative relationship η_∞(Re) is missing in literature.

This lack of information is related to the stability of Taylor bubbles. Goldsmith and Mason [11] found that the trailing end develops re-entrant cavities of the continuous liquid phase for high bubble speeds. For low Reynolds number, the corresponding re-entrant jet may cause bubble breakup at Ca ∼ 4−7 as experimentally observed by Olbricht and Kung [12] and confirmed by inertia-less numerical simulations by Lac and Sherwood [13], see also [50]. As the Reynolds number increases, the bubble might lose its axial symmetry at the rear. Water/nitrogen experiments in a 2 mm capillary by Asadolahi et al. [52] show that three-dimensional shape oscillations occur for Reyn-

olds numbers above Re ∼ 951 even for capillary numbers as low as Ca ∼ 0.007.

Predicting Taylor Flow Hydrodynamics

Among the quantities that are related to the characteristic velocity ratio η are the mean liquid velocity, the relative velocity, the gas hold-up, the cross-sectional area of the partial bypass flow and recirculation flow regions, the non-dimensional recirculation time in the liquid slug, the thickness of the liquid film and the bubble diameter. Table 1 summarizes the mathematical relations of these and further quantities with the characteristic velocity ratio. When the pipe radius, the gas and liquid flow rates and the physical properties of the phases are known, then j_T, β, Ca and Re are known as well. The correlation $\eta = \eta$(Ca, Re) given by Eqs. (33), (37) and (38) developed in this paper then links all priori unknown parameters in Tab. 1 with prior known parameters. Thus, the new model allows predicting a comprehensive set of hydrodynamic parameters characterizing gas-liquid Taylor flow in circular microchannels by one single relation.

By means of the identities $Ca_b = \eta$ Ca, $Re_b = \eta$ Re and $We_b = \eta^2 CaRe$, the proposed correlation can also be used to estimate the liquid film thickness or the pressure drop from correlations relying on Ca_b, Re_b and We_b, cf. the section with literature relations. Fur-

thermore, it is of benefit for modeling mass transfer in Taylor flow [53], as it allows estimating the streamline pattern in the liquid slug including the size of the recirculation area and the non-dimensional recirculation time, given in Eqs. (7) and (8), from prior known parameters.

The two-parameter logistic function in Eq. (33) with its asymptotic behavior at low capillary numbers agreeing with the theory of Bretherton [24], may also serve as basis for the development of correlations for a broader range of Taylor flow. While the present study is limited to gas-liquid flows, where the viscosity ratio λ approaches zero, the underlying approach could be applied to liquid-liquid flow as well. In literature, there exist already several numerical studies on liquid-liquid Taylor flows, which may serve as starting basis [34, 54–57]. Further potential extensions may concern larger/non-circular channels with upward/downward Taylor flow [18, 58]. In such cases, gravity/buoyancy forces are no longer negligible so that their influence on the characteristic velocity ratio should be taken into account by the Eötvös or Bond number.

CONCLUSIONS

Many hydrodynamic parameters of Taylor flow closely relate to the ratio between bubble velocity (u_b) and total superficial velocity (j_T). Correlations for this characteristic velocity ratio ($\eta = u_b/j_T$), which are valid in the entire range of capillary numbers, have been lacking so far. Using available theoretical, experimental and numerical results on gas-liquid Taylor flow in circular microchannels from literature, a correlation for η is proposed in terms of the capillary number (Ca) and Reynolds number (Re) both using j_T as velocity scale.

As basis for the correlation a five parameter logistic function is selected which accounts for the lower and upper asymptotes of η for small and large values of Ca while allowing for asymmetry. At low Ca, the correlation adopts the theoretical asymptotic limit of Bretherton resulting in excellent agreement with literature data. By this asymptotic behavior, the number of free parameters is reduced to two. One parameter is the value of the upper asymptote while the other one accounts for the asymmetry of the logistic curve. Both remaining free parameters are obtained by regression analysis using numerical simulation data for η from literature. The new correlation is given by Eqs. (33), (37) and (38). The deviation between the correlation and numerical data for Re up to 800 is within $\pm 5\%$ over the entire range of Ca. In comparison with experimental data, the agreement is less good but still within $\pm 18\%$.

For large values of Ca and Re, a further improvement of the new model is desirable. In literature there is, however, a relative large uncertainty concerning the upper asymptote of the characteristic velocity ratio for finite Reynolds number. Here, numerical studies where Ca and Re can be varied independently may be particularly useful to determine not only the upper asymptote but also the upper value of Ca where the Taylor bubble shape is stable for certain finite values of Re.

Since the proposed correlation relies on prior knowledge of physical properties and gas/liquid flow rates only, it should be particularly useful to predict hydrodynamic attributes of Taylor flow such as bubble velocity, mean liquid velocity, gas holdup, uniform liquid film thickness, bubble diameter, and streamline patterns in the liquid slug. Furthermore, the present model can be used in combination with models for liquid film thickness or pressure drop formulated in terms of non-dimensional groups being based on the bubble velocity instead of total superficial velocity. Finally, the developed two-parameter logistic function may also serve as prototype for similar correlations valid for non-circular capillary channels and liquid-liquid Taylor flow.

NOTATION

A area, m^2

α void fraction (holdup)

Bo   Bond number

β gas volumetric flow ratio (dynamic holdup)

c parameter in 5PL function

Ca   capillary number based on total superficial velocity, $\mathrm{Ca} = j_T \mu_L/\sigma$

Ca_b capillary number based on bubble velocity, $\mathrm{Ca}_b = u_b \mu_L/\sigma$

D inner diameter of circular pipe, m

δ uniform liquid film thickness, m

Eo   Eötvös number

F constant parameter in Eq. (10)

g gravitational acceleration, m s^{-2}

h parameter in 5PL function

j_T total superficial velocity, m s^{-1}

λ gas-to-liquid viscosity ratio

m relative drift velocity

μ dynamic viscosity, Pa s

η characteristic velocity ratio, $\eta = u_b/j_T$

P constant in Bretherton model, $P = 1.3375$

Q volumetric flow rate, $m^3\ s^{-1}$

R pipe radius, m

R_b uniform bubble radius, m

Re   Reynolds number based on total superficial velocity, $Re = \rho_L j_T D/\mu_L$

Re_b Reynolds number based on bubble velocity, $Re_b = \rho_L u_b D/\mu_L$

s parameter in 5PL function

ρ density, $kg\ m^{-3}$

S slip ratio

σ coefficient of surface tension, $N\ m^{-1}$

τ dimensionless recirculation time

u_b bubble velocity, $m\ s^{-1}$

u_d drift velocity, $m\ s^{-1}$

u_L mean liquid velocity, $m\ s^{-1}$

w wetting fraction

We   Weber number

SUBSCRIPTS

b bubble

f film

G gas

L liquid

s slug

T total

0   asymptotic value at zero capillary number

∞ asymptotic value at large capillary number

ABBREVIATIONS

5PL   five-parameter logistic (function)

CBF   complete bypass flow

ds   dividing streamline

SFA   stagnant film assumption

REFERENCES

1. Kreutzer, M.T., Kapteijn, F., Moulijn, J.A., and Heiszwolf, J.J., Multiphase monolith reactors: Chemical reaction engineering of segmented flow in microchannels, *Chem. Eng. Sci.*, 2005, vol. 60, no. 22, p. 5895.

2. Triplett, K.A., Ghiaasiaan, S.M., Abdel-Khalik, S.I., and Sadowski, D.L., Gas-liquid two-phase flow in microchannels—Part I: Two-phase flow patterns, *Int. J. Multiphase Flow*, 1999, vol. 25, no. 3, p. 377.

3. Günther, A., Jhunjhunwala, M., Thalmann, M., Schmidt, M.A., and Jensen, K.F., Micromixing of miscible liquids in segmented gas-liquid flow, *Langmuir*, 2005, vol. 21, no. 4, p. 1547.

4. Haase, S., Murzin, D.Y., and Salmi, T., Review on hydrodynamics and mass transfer in minichannel wall reactors with gas-liquid Taylor flow, *Chem. Eng. Res. Des.*, 2016, vol. 113, p. 304.

5. Abiev, R., Svetlov, S., and Haase, S., Hydrodynamics and mass transfer of gas-liquid and liquid-liquid Taylor flow in microchannels, *Chem. Eng. Technol.*, 2017, vol. 40, no. 11, p. 1985.

6. Angeli, P. and Gavriilidis, A., Hydrodynamics of Taylor flow in small channels: A review, *Proc. Inst. Mech. Eng., Part C*, 2008, vol. 222, no. 5, p. 737.

7. Howard, J.A. and Walsh, P.A., Review and extensions to film thickness and relative bubble drift velocity prediction methods in laminar Taylor or slug flows, *Int. J. Multiphase Flow*, 2013, vol. 55, p. 32.

8. Giavedoni, M.D. and Saita, F.A., The axisymmetric and plane cases of a gas phase steadily displacing a Newtonian liquid—A simultaneous solution of the governing equations, *Phys. Fluids*, 1997, vol. 9, no. 8, p. 2420.

9. Magnini, M., Ferrari, A., Thome, J.R., and Stone, H.A., Undulations on the surface of elongated bubbles in confined gas-liquid flows, *Phys. Rev. Fluids*, 2017, vol. 2, no. 8, p. 084001.

10. Giavedoni, M.D. and Saita, F.A., The rear meniscus of a long bubble steadily displacing a Newtonian liquid in a capillary tube, *Phys. Fluids*, 1999, vol. 11, no. 4, p. 786.

11. Goldsmith, H.L. and Mason, S.G., Flow of suspensions through tubes. II. Single large bubbles, *J. Colloid Sci.*, 1963, vol. 18, no. 3, p. 237.

12. Olbricht, W.L. and Kung, D.M., The deformation and breakup of liquid-drops in low Reynolds-number flow through a capillary, *Phys. Fluids A*, 1992, vol. 4, no. 7, p. 1347.

13. Lac, E. and Sherwood, J.D., Motion of a drop along the centreline of a capillary in a pressure-driven flow, *J. Fluid Mech.*, 2009, vol. 640, p. 27.

14. Suo, M. and Griffith, P., Two-phase flow in capillary tubes, *J. Basic Eng.*, 1964, vol. 86, no. 3, p. 576.

15. Wörner, M., A key parameter to characterize Taylor flow in narrow circular and rectangular channels, *7th International Conference on Multiphase Flow (ICMF 2010)*, Gainesville, Fla.: Univ. of Florida, 2010,

16. Lizarraga-Garcia, E., Buongiorno, J., Al-Safran, E., and Lakehal, D., A broadly-applicable unified closure relation for Taylor bubble rise velocity in pipes with stagnant liquid, *Int. J. Multiphase Flow*, 2017, vol. 89, p. 345.

17. Leung, S.S.Y., Gupta, R., Fletcher, D.F., and Haynes, B.S., Gravitational effect on Taylor flow in horizontal microchannels, *Chem. Eng. Sci.*, 2012, vol. 69, no. 1, p. 553.

18. Magnini, M., Khodaparast, S., Matar, O.K., Stone, H.A., and Thome, J.R., Dynamics of long gas bubbles rising

in a vertical tube in a cocurrent liquid flow, *Phys. Rev. Fluids*, 2019, vol. 4, no. 2, p. 023601.

19. Schwartz, L.W., Princen, H.M., and Kiss, A.D., On the motion of bubbles in capillary tubes, *J. Fluid Mech.*, 1986, vol. 172, p. 259.

20. Cherukumudi, A., Klaseboer, E., Khan, S.A., and Manica, R., Prediction of the shape and pressure drop of Taylor bubbles in circular tubes, *Microfluid. Nanofluid.*, 2015, vol. 19, no. 5, p. 1221.

21. Kurimoto, R., Nakazawa, K., Minagawa, H., and Yasuda, T., Prediction models of void fraction and pressure drop for gas-liquid slug flow in microchannels, *Exp. Therm. Fluid Sci.*, 2017, vol. 88, p. 124.

22. Abiev, R.S., Simulation of the slug flow of a gas-liquid system in capillaries, *Theor. Found. Chem. Eng.*, 2008, vol. 42, no. 2, p. 105.

23. Taylor, G.I., Deposition of a viscous fluid on the wall of a tube, *J. Fluid Mech.*, 1961, vol. 10, no. 2, p. 161.

24. Bretherton, F.P., The motion of long bubbles in tubes, *J. Fluid Mech.*, 1961, vol. 10, no. 2, p. 166.

25. Reinelt, D.A. and Saffman, P.G., The penetration of a finger into a viscous-fluid in a channel and tube, *SIAM J. Sci. Stat. Comp.*, 1985, vol. 6, no. 3, p. 542.

26. Shen, E.I. and Udell, K.S., A finite-element study of low Reynolds-number two-phase flow in cylindrical-tubes, *J. Appl. Mech.*, 1985, vol. 52, no. 2, p. 253.

27. Halpern, D. and Gaver, D.P., Boundary-element analysis of the time-dependent motion of a semiinfinite bubble in a channel, *J. Comput. Phys.*, 1994, vol. 115, no. 2, p. 366.

28. Martinez, M.J. and Udell, K.S., Boundary integral analysis of the creeping flow of long bubbles in capillaries, *J. Appl. Mech.*, 1989, vol. 56, no. 1, p. 211.

29. Cox, B.G., An experimental investigation of the streamlines in viscous fluid expelled from a tube, *J. Fluid Mech.*, 1964, vol. 20, no. 2, p. 193.

30. Thulasidas, T.C., Abraham, M.A., and Cerro, R.L., Flow patterns in liquid slugs during bubble-train flow inside capillaries, *Chem. Eng. Sci.*, 1997, vol. 52, no. 17, p. 2947.

31. Kececi, S., Wörner, M., Onea, A., and Soyhan, H.S., Recirculation time and liquid slug mass transfer in co-current upward and downward Taylor flow, *Catal. Today*, 2009, vol. 147S, p. S125.

32. Aussillous, P. and Quere, D., Quick deposition of a fluid on the wall of a tube, *Phys. Fluids*, 2000, vol. 12, no. 10, p. 2367.

33. Klaseboer, E., Gupta, R., and Manica, R., An extended Bretherton model for long Taylor bubbles at moderate capillary numbers, *Phys. Fluids*, 2014, vol. 26, no. 3, p. 032107.

34. Balestra, G., Zhu, L., and Gallaire, F., Viscous Taylor droplets in axisymmetric and planar tubes: From Bretherton's theory to empirical models, *Microfluid. Nanofluid.*, 2018, vol. 22, no. 6, p. 67.

35. de Ryck, A., The effect of weak inertia on the emptying of a tube, *Phys. Fluids*, 2002, vol. 14, no. 7, p. 2102.

36. Heil, M., Finite Reynolds number effects in the Bretherton problem, *Phys. Fluids*, 2001, vol. 13, no. 9, p. 2517.

37. Han, Y. and Shikazono, N., Measurement of the liquid film thickness in micro tube slug flow, *Int. J. Heat Fluid Flow*, 2009, vol. 30, no. 5, p. 842.

38. Langewisch, D.R. and Buongiorno, J., Prediction of film thickness, bubble velocity, and pressure drop for capillary slug flow using a CFD-generated database, *Int. J. Heat Fluid Flow*, 2015, vol. 54, p. 250.

39. Kurimoto, R., Hayashi, K., Minagawa, H., and Tomiyama, A., Numerical investigation of bubble shape and flow field of gas—liquid slug flow in circular microchannels, *Int. J. Heat Fluid Flow*, 2018, vol. 74, p. 28.

40. Fairbrother, F. and Stubbs, A.E., Studies in electro-endosmosis. Part VI. The "bubble-tube" method of measurement, *J. Chem. Soc.*, 1935, p. 527.

41. Liu, H., Vandu, C.O., and Krishna, R., Hydrodynamics of Taylor flow in vertical capillaries: Flow regimes, bubble rise velocity, liquid slug length, and pressure drop, *Ind. Eng. Chem. Res.*, 2005, vol. 44, no. 14, p. 4884.

42. Kreutzer, M.T., Kapteijn, F., Moulijn, J.A., Kleijn, C.R., and Heiszwolf, J.J., Inertial and interfacial effects on pressure drop of Taylor flow in capillaries, *AlChE J.*, 2005, vol. 51, no. 9, p. 2428.

43. Abiev, R.S., Bubbles velocity, Taylor circulation rate and mass transfer model for slug flow in milli- and microchannels, *Chem. Eng. J.*, 2013, vol. 227, p. 66.

44. Zuber, N. and Findlay, J.A., Average volumetric concentration in two-phase flow systems, *J. Heat Transfer*, 1965, vol. 87, no. 4, p. 453.

45. Nicklin, D.J., Wilke, J.O., and Davidson, J.F., Two-phase flow in vertical tubes, *Trans. Inst. Chem. Eng.*, 1962, vol. 40, p. 61.

46. Yuster, S.T., Theoretical considerations of multiphase flow in idealized capillary systems, *Proceedings of the Third World Petroleum Congress. Section II. Drilling and Production,* Schurink, H.B.J. et al., Eds., Leiden: E.J. Brill, 1951, p. 437.

47. Russell, T.W.F. and Charles, M.E., The effect of the less viscous liquid in the laminar flow of two immiscible liquids, *Can. J. Chem. Eng.*, 1959, vol. 37, no. 1, p. 18.

48. Makuch, K., Gorce, J.-B., and Garstecki, P., Non-wetting droplets in capillaries of circular cross-section: Scaling function, *Phys. Fluids*, 2019, vol. 31, no. 4, p. 043102.

49. Cox, B.G., On driving a viscous fluid out of a tube, *J. Fluid Mech.*, 1962, vol. 14, no. 1, p. 81.

50. Dupont, J.-B., Legendre, D., and Fabre, J., Motion and shape of long bubbles in small tube at low Re-number, *International Conference on Multiphase Flow (ICMF 2007),* Sommerfeld, M., Ed., Leipzig, 2007.

51. Gottschalk, P.G. and Dunn, J.R., The five-parameter logistic: A characterization and comparison with the four-parameter logistic, *Anal. Biochem.*, 2005, vol. 343, no. 1, p. 54.

52. Asadolahi, A.N., Gupta, R., Leung, S.S.Y., Fletcher, D.F., and Haynes, B.S., Validation of a CFD model of Taylor flow hydrodynamics and heat transfer, *Chem. Eng. Sci.*, 2012, vol. 69, no. 1, p. 541.

53. Butler, C., Cid, E., and Billet, A.M., Modelling of mass transfer in Taylor flow: Investigation with the PLIF-I technique, *Chem. Eng. Res. Des.*, 2016, vol. 115, p. 292.

54. Carroll, R.M. and Gupta, N.R., Inertial and surfactant effects on the steady droplet flow in cylindrical channels, *Phys. Fluids*, 2014, vol. 26, no. 12, p. 122102.

55. Khodaparast, S., Magnini, M., Borhani, N., and Thome, J.R., Dynamics of isolated confined air bubbles in liquid flows through circular microchannels: An experimental and numerical study, *Microfluid. Nanofluid.*, 2015, vol. 19, no. 1, p. 209.

56. Soares, E.J., Thompson, R.L., and Niero, D.C., Immiscible liquid−liquid pressure-driven flow in capillary tubes: Experimental results and numerical comparison, *Phys. Fluids*, 2015, vol. 27, no. 8, p. 082105.

57. Abiev, R.S. and Dymov, A.V., Modeling the hydrodynamics of slug flow in a minichannel for liquid-liquid two-phase system, *Theor. Found. Chem. Eng.*, 2013, vol. 47, no. 4, p. 299.

58. Keskin, Ö., Wörner, M., Soyhan, H.S., Bauer, T., Deutschmann, O., and Lange, R., Viscous co-current downward Taylor flow in a square mini-channel, *AIChE J.*, 2010, vol. 56, no. 7, p. 1693.